JACS Au
AN OPEN ACCESS JOURNAL OF THE AMERICAN CHEMICAL SOCIETY

pubs.acs.org/jacsau

Article

Graphene Oxide as a Pb(II) Separation Medium: Has Part of the Story Been Overlooked?

Manh-Thuong Nguyen, Jun Zhang, Venkateshkumar Prabhakaran, Shuai Tan, Eric T. Baxter, Vaithiyalingam Shutthanandan, Grant E. Johnson,* Roger Rousseau, and Vassiliki-Alexandra Glezakou*

Cite This: *JACS Au* 2021, 1, 766–776

Read Online

ACCESS | Metrics & More | Article Recommendations | Supporting Information

ABSTRACT: A key problem associated with the design of graphene oxide (GO) materials and their tuning for nanoscale separations is how specific functional groups influence the competitive adsorption of solvated ions and water at liquid/graphene interfaces. Computation accompanied by experiment shows that OH and COOH exert an influence on water adsorption properties stronger than that of O and H functional groups. The COO^- anions, following COOH deprotonation, stabilize Pb(II) through strong electrostatic interactions. This suggests that, among the functional groups under study, COOH offers the best Pb(II) adsorption capacity and the ability to regenerate the sorbent through a pH swing. In line with computation, striking experimental observations revealed that a substantial increase in Pb(II) adsorption occurs with increasing pH. Our findings provide a systematic framework for controlled design and implementation of regenerable C-based sorbents used in separations and desalination.

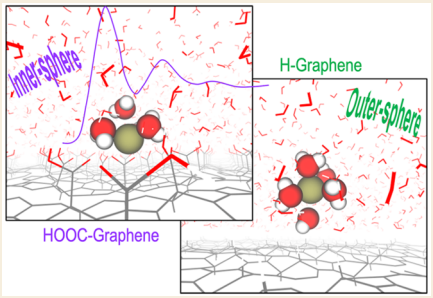

KEYWORDS: *Graphene oxide, membrane separation, ion transport, lead removal, adsorption, desorption, pH, AIMD*

INTRODUCTION

The lead ion (Pb(II)) is a typical representative of heavy metal ions in water. Considered as one of the most toxic kinds of ions, Pb(II) can severely harm human bodies. Therefore, the efficient separation/removal of Pb(II) from aqueous solutions is highly important and has attracted much attention.[1−4] In particular, Pb(II) separation using graphene oxide (GO) is the subject of numerous investigations. In separation technologies, GO has been shown to be a highly promising material,[5,6] used for gas and ion separation,[5,7−9] water purification, and desalination,[10−12] with outstanding efficiency. High surface area (700 m^2/g or more[13]) and high cation adsorption affinity make GO an excellent material for cation removal/separation. GO is easy to prepare in scalable quantities and may be fabricated or assembled into laminate structures with controlled interlayer distances at the nanometer scale. This stacked laminate structure allows water molecules to permeate through the interconnected network formed by GO nanosheets.[12] The high surface area in the transport channels ensures that a high water flux can be achieved.[14] By adjusting the GO spacing through sandwiching appropriately sized spacers between GO nanosheets, a broad spectrum of GO membranes can be made, each being able to precisely separate target ions and molecules within a specific size range from bulk solution.[15] Various types of heavy ions can form stable surface complexes with GO, making GO an adsorbent to remove these ions from aqueous solutions. This is typically the case for Pb(II) ions.[5,6] Li et al. show that mesoporous silica-grafted graphene oxide materials have high capacity for Pb(II) adsorption.[16] In an aqueous solution, the adsorption rate of Pb(II) on these materials is 2 orders higher than that of Li(I). The maximum Pb(II) adsorption capacity of these materials peaks at 255 mg/g in the 4−7 pH range.

In separations, as well as in other applications such as catalysis or electronics, GO is a much better material than graphene.[17] Whereas the surface of graphene is highly hydrophobic,[18] surfaces of GO are hydrophilic.[19,20] Because graphene is chemically inert, its chemical reactivity is mainly attributed to the π electron system. Computational studies show that the interactions between graphene and molecules are weak[21,22] and are mostly dominated by van der Waals interactions.[22] Similarly, interactions between ions and graphene, known as ion−π interactions, are also weak albeit of electrostatic nature.[23] GO, on the other hand, offers much better chemical capacity. O-containing functional groups, which are usually strongly polarized, with electron lone pairs act as active sites for the adsorption of molecules or atoms.[24] The superior performance of GO versus that of pristine graphene in the adsorption of metal cations has been demonstrated in various studies. For instance, GO has an adsorption capacity for Cu(II) 10 times higher than that of

Received: November 21, 2020
Published: April 5, 2021

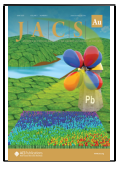

https://doi.org/10.1021/jacsau.0c00075
JACS Au 2021, 1, 766–776

active carbon,[25] and an oxidized graphene sheet has a Pb(II) adsorption capacity 2 times higher than that of pristine graphene.[26] GO, commonly prepared by chemical oxidation of graphite and subsequent exfoliation,[27] contains various functional groups such as O, OH, COOH, or H. Due to their intrinsic difference in polarizability, these groups exhibit different adsorption strengths toward metal cations. For Pb(II) adsorption, Huang et al. hypothesized the important role of COOH groups over other O-containing functional groups.[26] Also for Pb(II) adsorption, density functional theory (DFT) calculations predict that Pb(II) binds more strongly to COOH groups than to O groups.[28] This implies that the chemical composition of GO is a key factor in controlling the adsorption capacity of GO. Although there are numerous studies dedicated to understanding effects of ionic strength[29] or the pH of solution,[28,29] on the adsorption of metal cations on GO, much less is known, especially at a molecular level, about the influence of each different functional group.

In the adsorption of metal cations on GO, water certainly plays an important role. Generally speaking, by solvation and competitive adsorption, water weakens the interaction between GO and the ions. This has been seen in the adsorption phenomenon in many systems such as organics on solid surfaces[30] or CO_2 in metal−organic frameworks.[31] As the hydration free energy of Pb(II) is relatively high, −1425 kJ/mol,[32] water certainly changes the adsorption strength of GO toward Pb(II). Furthermore, ion separation using GO membranes is significantly influenced by the distance between GO layers as well as the adsorption and transport of ions through interlayer spaces of GO.[11,33] In an aqueous solution, GO is also solvated, and this distance is changed by hydrogen bonds and electrostatic interactions between water and functional groups.[34] How well water would solvate GO essentially depends on the chemical composition of GO. Nevertheless, the influence of individual functional groups on the interaction of GO and a water solution has not been understood yet. From a computational point of view, liquid/GO interfaces represent a group of highly complex systems which are not adequately modeled through simple static optimization methods. Static DFT calculations can provide information about the adsorption energy of the adsorbate in the gas phase.[28] Nevertheless, to understand the chemistry/physics underlying a separation process, the dynamics of solvents, the solvation, and the desolvation at the interface, the speciation, together with the competitive adsorption between water and cations in the system, must be addressed. This can only be done by applying statistical mechanics-based approaches with reactive potentials (e.g., DFT) to liquid/solid systems. Very little has been done regarding this aspect.

Herein, we examine the reversible adsorption and diffusion of Pb(II) through GO laminate membranes containing specific surface oxygen functional groups by means of ab initio molecular dynamics (AIMD) simulations and a combination of experimental techniques. We modulate the surface functionality of GO by conducting Pb adsorption experiments at different pH values (3 to 7). We explore whether lower pH conditions protonate −COOH groups and higher pH values deprotonate them ($-COO^-$), thereby making them available for adsorption of Pb(II) through formation of an electrostatic bond. The interaction of the COOH groups on GO with Pb(II), as well as the effect of deprotonation of −COOH on the adsorption of Pb(II), was first observed in molecular simulation and subsequently characterized using infrared, Raman, and X-ray photoelectron spectroscopy (XPS). The interlayer spacing of the GO laminates at different pH values was determined by X-ray diffraction (XRD). The permeation and diffusion of Pb(II) through the GO membranes was determined by simulation and electrochemically using an ion selective electrode and electrochemical impedance spectroscopy.

RESULTS AND DISCUSSION

In this section, we will discuss the structure and dynamics of our systems through analysis of the molecular trajectories. Details about the simulation systems can be found in the "Computational Methods" section at the end of the article.

Statistical Analysis of Molecular Trajectories

Water Density. Figure 1 shows the water density against the distance to carbon planes of functionalized graphene

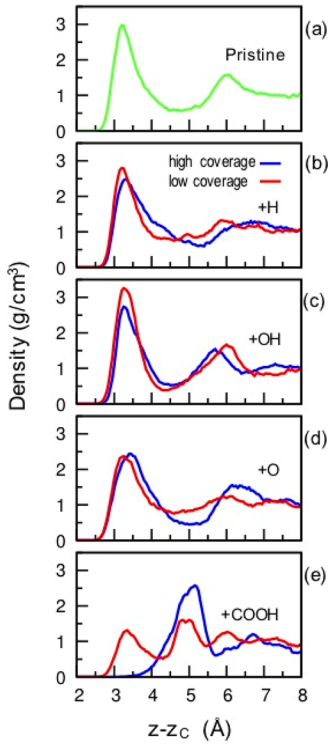

Figure 1. (a−e) Density of water versus local height relative to C atoms of the C plane.

sheets. Consistent with previous works,[35] the first peak is located at 3.1 Å while the second peak is at 6 Å (Figure 1a). On reduced graphene (H-graphene) while at low coverage (see Methods and section S1), the first peak height and position are not changed much compared to the pristine graphene case; at high coverage, both first and second peaks change in shape and shift further their positions (Figure 1b). On oxidized graphene (HO-graphene) at low coverage, the water density in the first layer is the highest of all cases, whereas at high coverage, it is similar to that on pristine graphene. On O-graphene, the first peak is lower and broader compared to that on pristine graphene; high coverage leads to a flatter second peak. Finally, on HOOC-graphene, the density changes significantly compared to the previous cases. At high coverage, the first peak is at 5 Å because the higher −COOH density does not leave enough space between the functional groups for water

https://doi.org/10.1021/jacsau.0c00075
JACS Au 2021, 1, 766−776

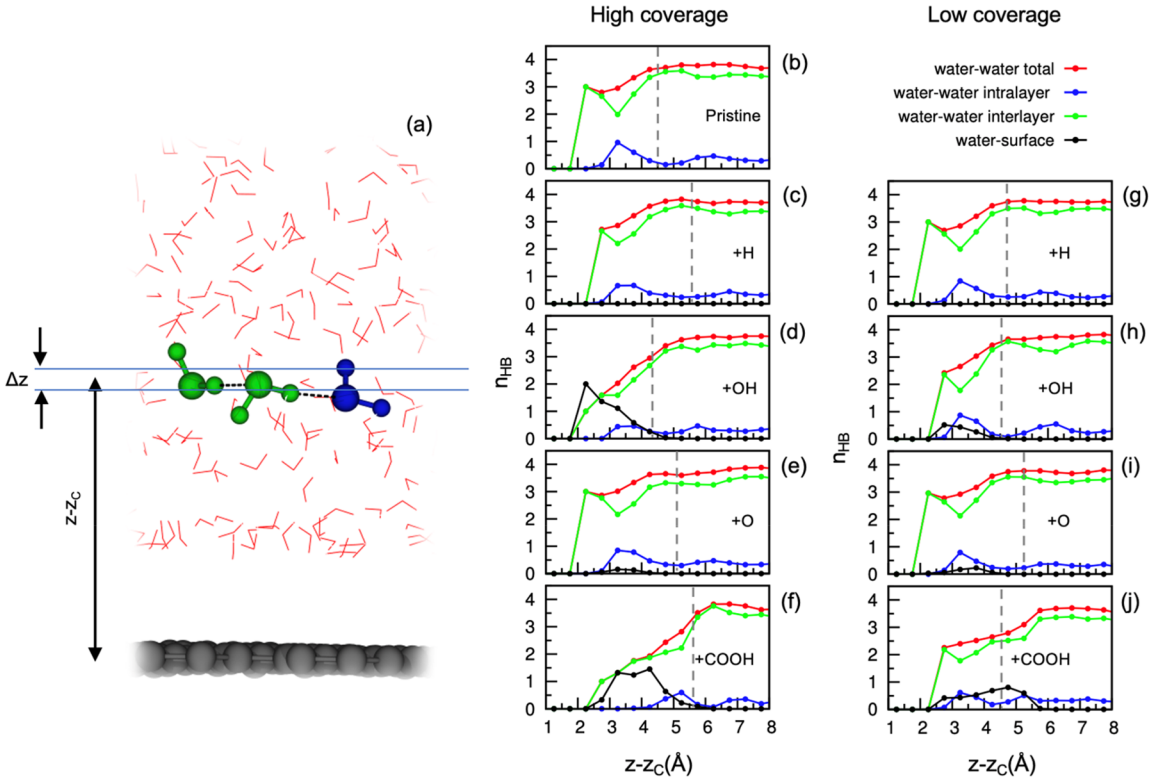

Figure 2. (a) Slice (layer) of water of thickness Δz at the distance z from the carbon surface. Water molecules in green show an intralayer HB, whereas a water molecule in green and one in blue show an interlayer HB. (b–j) Number of HBs per water molecule versus the distance to the carbon surface, at different coverage and functionalization. The water–water HBs are from water in the same or different layers, and the thickness of each layer here is chosen at 0.5 Å. Dashed lines indicate the first minimum positions in the density profiles in Figure 1.

molecules to approach the carbon plane, even though the tail of the water density peak toward the surface is longer than that in other cases. The water density profiles suggest that water molecules on low-coverage HOOC-graphene can desorb more easily (section S2) and have lower coordination number (section S3) than on other surfaces.

Number of Hydrogen Bonds (HBs). The HBs here are categorized into intralayer and interlayer contributions,[36] and each "layer" in this context is defined as a "water slice" of 0.5 Å thickness (Figure 2a). As shown below, the number of intralayer HBs is strongly affected by the water density.

On pristine graphene, the number of intralayer HBs anticorrelates with the number of interlayer HBs (Figure 2b). In agreement with previous studies, the number of HBs per molecule in the interfacial layer is within the range of 3 to 3.6,[35] whereas in the water bulk region (>8 Å from the graphene surface), it is about 3.5.[37]

On H-graphene, low coverage has little effect on the total number of HBs, wherease higher coverage increases it (Figure 2c,g), consistent with the higher water coordination number in the case of the high coverage (see section S3). No water–surface HBs were found.

On HO-graphene, −OH groups increase the number of intralayer HBs (Figure 2d,h). Here, the water–surface HBs play an important role as both the hydroxyl groups and the water molecules have acceptor and donor sites. Interestingly, at high coverage, in the layer closest to the surface, the total number of water–water HBs is lower than the number of water–surface HBs.

On O-graphene (Figure 2e,i), it is very similar to H-graphene. Here though, the H atoms of water point downward to the surface, forcing the waters to be less parallel to the surface, thereby reducing the number of intramolecular HBs. Nevertheless, the number of HBs is lower than in the case of OH-graphene, partly because O-graphene has only acceptor sites for HBs.

Similar to the HO-graphene case, on HOOC-graphene, the number of water–water HBs is lower than that in the cases of pristine, O-, and H-graphene, as the water–surface HBs are prevalent (Figure 2f,j).

Although these results are not surprising given the hydrophilic nature of −COOH and −OH groups and hydrophobic nature of pristine and −H-functionalized graphene, they are counterintuitive in the case of O-graphene, whose interfacial structure is in closer alignment with the more hydrophobic systems. This conclusion is further supported by the orientation (section S4), diffusion, and relaxation times (section S5) of water in the first layer at the interface. The findings of this analysis show that at the hydrophilic surfaces (−OH and −COOH) the diffusion of water in the interfacial layer decreases to $\sim 1.6 \times 10^{-5}$ cm^2/s, while the residence times increase, indicating interfacial dynamics slower than those of hydropohobic surfaces. In addition, the water polarizability and acting forces by the surface were calculated using maximally localized Wannier functions (section S6), further asserting the difference of the surface functionalization on the water transport at the interface (section S5). The strong polarization of water and vertical forces induced by the hydrophilic −OH and −COOH groups result in asymmetric force distributions due to strong hydrogen bonding (section S6), which is in part attributed to the large atomic charges in the functional groups (section S1).

https://doi.org/10.1021/jacsau.0c00075
JACS Au 2021, 1, 766–776

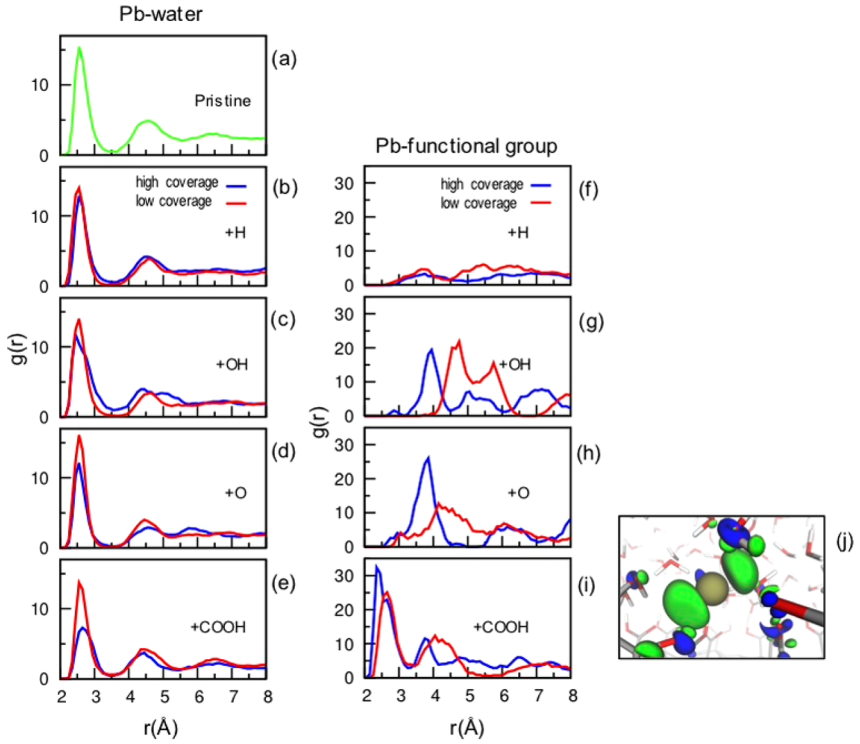

Figure 3. (a–e) Radial distribution function of the Pb–O pairs (O of water). (f–i) Radial distribution of Pb–X pairs (X of functional groups, X = H in H functionalization, X = O in O, OH, HOOC, functionalization). (j) Bonding charge density difference (defined as the difference in the change density of the whole system minus that of isolated Pb(II) and the remaining components) at the isosurface value of 0.01 au from a frame in the high-coverage COOH-graphene simulation.

Pb(II) Adsorption. The adsorption of Pb(II) changes significantly from one surface to another (Figures 3 and S7). The broad distribution of Pb(II) on the pristine or H-graphene and narrow distribution of Pb(II) on O-, HO-, and HOOC-graphene surfaces suggest that Pb(II) is more strongly bound to O-containing surfaces. Additionally, the functional coverage also affects the distribution of Pb(II). On pristine and H-graphene, the distribution of Pb(II) (Figure S7a,b) is diffuse, indicating that Pb(II) is likely to move freely at these interfaces. On HO-, O-, and HOOC-graphene, well-defined distributions were found (Figure S7c–e) due to the strong interactions between Pb(II) and the hydroxyl, epoxy, and carboxylic groups. In all of these three cases, Pb(II) has well-formed distributions with peak values at ∼4–5 Å depending on the coverage. Details of coordination number changed with functionality are provided in section S8.

The interaction between Pb(II) and the conjugated π-electron-rich system graphene surface is electrostatic in nature.[38] In an aqueous environment, this interaction is shielded by the solvation shell of the cation, resulting in minimal interaction, as indicated in the distribution of Pb(II) (Figure S7a). Except for high-coverage HOOC-graphene, the dominant solvation interactions between Pb and water are similar across the different substrates or degree of functionalization (Figure 3a–e). The first solvation shell has a maximum at ∼2.6 Å and the second shell at 4.5 Å. The coordination number slightly increases to ∼7 at the interface compared to 6.6 in bulk water.

Finally, we looked at the radial distribution function (RDF) between Pb(II) and the functional groups (Figure 3f–i). Not surprisingly, the O-bearing functionalization has the biggest effect on the Pb RDFs and hydration structure. However, it is clear that in the case of −OH and −O, the Pb functional group interaction is distinctly weaker, with Pb−O_{func} ∼ 4 Å or higher, with Pb showing two distinct hydration shells. This is consistent with the formation of outer-sphere Pb−aqua complexes. In the case of −COOH, the Pb−O_{func} distance is much shorter with the first max of the RDF at ∼2.5 Å, which is indicative of a direct Pb−O_{func} bond and inner-sphere coordination complex (Figure 3i). This is consistent with other reported values of first coordination Pb−O distances in the literature.[39] The strong bond in this case is further demonstrated with the bonding charge density (Figure 3j; also see section S9). This is also reflected in the extended solvation structure of Pb(II), exhibiting three solvation shells within 8 Å (Figure 3e). These stable complexes of Pb are critical in impacting the diffusion of Pb at the interface, by retarding the cation diffusion by 1–2 orders of magnitude relative to pristine graphene; see section S10 and Table S4 in the Supporting Information.

HOOC-graphene is the most prominent example of how chemical functionalization would affect the adsorption behavior of Pb(II) from an aqueous solution on graphene. Closely following the structure in the vicinity of Pb(II), we observe the deprotonation of a −COOH group, resulting in a carboxylate anion interacting with Pb(II) and a hydronium molecule (section S11). This suggests that the adsorption strength of Pb(II) on HOOC-graphene can be controlled by the pH of the solution, which can also be used as a pH swing for the adsorption/desorption of cations.[26]

https://doi.org/10.1021/jacsau.0c00075
JACS Au 2021, 1, 766–776

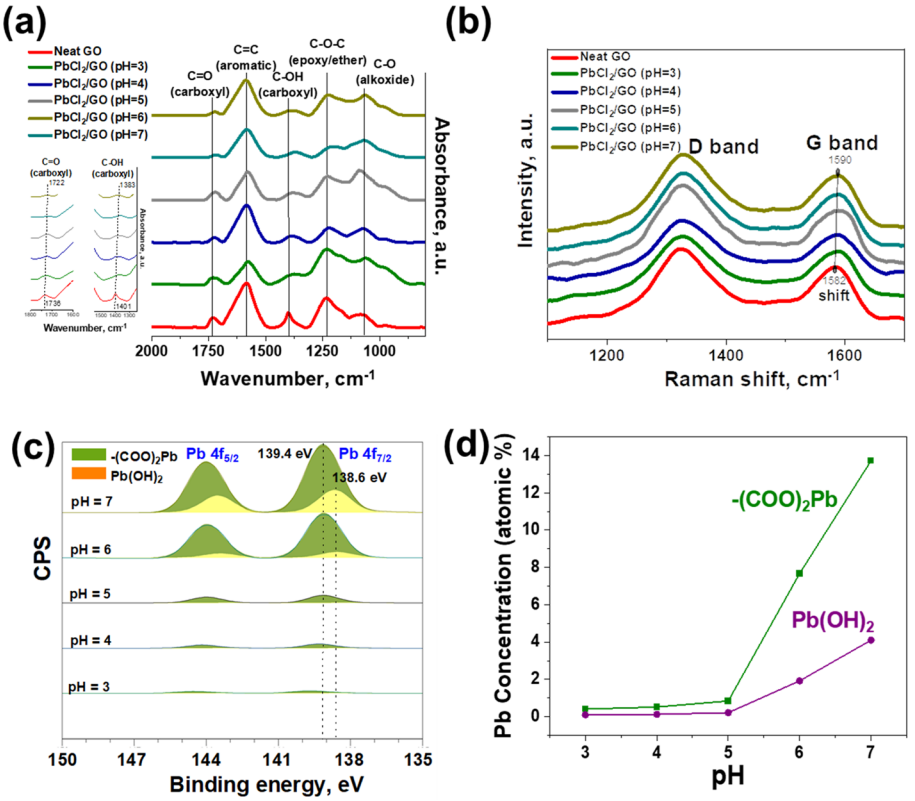

Figure 4. (a) FTIR spectra of GO membranes filtered with $PbCl_2$ solution at different pH (3−7). Inset: FTIR spectra of carboxyl C−OH and C═O bands on GO showing peak shifts as a function of increasing pH; (b) Raman spectra of GO membranes filtered with $PbCl_2$ solution at different pH showing the shift of the G band as a function of increasing pH; (c,d) Pb 4f XPS spectra and corresponding Pb atomic concentration determined from GO membranes filtered with $PbCl_2$ solution at different pH showing an increase in Pb adsorption with higher pH.

Experimental Determination of Reversible Pb(II) Adsorption and Diffusion through Functionalized GO Membranes

To validate our theoretical predictions, we experimentally studied the reversible adsorption and diffusion of Pb(II) through GO membranes with different functionality. For the Pb(II) adsorption experiments, we modulated the functionality of GO by conducting experiments at different pH (3−7). We anticipated that lower pH will protonate −COOH groups, whereas higher pH will deprotonate them ($-COO^-$), making them available for Pb(II) adsorption. The interaction of −COOH groups with Pb(II) and the effect of deprotonation on adsorption were characterized using Fourier transform infrared (FTIR), Raman, and XPS (Figures 4 and S12−S16).

Coordination of Pb(II) by COOH groups was observed as peak shifts in the IR[40] and Raman spectra (Figure 4a,b).[41] The carboxyl C−OH (1401 cm^{-1}) and C═O (1736 cm^{-1}) peaks in neat GO were red-shifted to 1383 and 1722 cm^{-1} in $PbCl_2$/GO (pH = 7), respectively. The G band of GO was shifted from 1582 cm^{-1} in neat GO to 1590 cm^{-1} in $PbCl_2$/GO (pH = 7), likely due to electron transfer and/or physical stress on the GO sheet cross-linked by $-(COO)_2Pb$ at the edges. XPS confirmed and quantified formation of $-(COO)_2Pb$ complexes on GO. In Figure S12, the C 1s XPS spectra were deconvoluted into five peaks at 283.8, 284.9, 286.9, 287.5, and 289 eV assigned to sp^2, sp^3 carbon, C−O, C═O, and −COOH, respectively. Increasing the pH of the $PbCl_2$ solution causes the C 1s electron binding energy of −COOH to shift higher (289.5 eV) than the corresponding $-(COO)_2Pb$ complex. The C 1s spectra also revealed that $PbCl_2$/GO (pH = 6 and 7) have lower intensities of C−C and C−O/C═O peaks than other GO membranes, likely resulting from layers of $Pb(OH)_2$ precipitate in basic $PbCl_2$ solutions, as indicated by the Pb 4f spectra. Formation of $-(COO)_2Pb$ complexes at increasing pH was confirmed by the major peak at 139.4 eV (Figure 4c).[42] By accounting for the Pb contribution from $Pb(OH)_2$, the atomic concentration of $-(COO)_2Pb$ was determined (Figure 4d), revealing a substantial increase from <1% in $PbCl_2$/GO (pH = 3) to 14% (pH = 7), which is attributed to more deprotonated COO^- groups available for Pb(II) adsorption. XPS imaging revealed spatial heterogeneity of the C−O and Pb distributions on GO at different pH, corroborating the increased Pb adsorption at higher pH (Figure S13).

The reversibility of Pb coordination by carboxyl acid groups was investigated by protonating the $-(COO)_2Pb$ complexes on GO by performing an acid wash on the $PbCl_2$/GO (pH = 5) with 1.05% Pb atomic concentration (Figure S14). After the acid wash, the atomic concentration of Pb decreased to <0.4%, indicating that Pb adsorbed on −COO desorbs through a pH-driven mechanism. The XPS results presented in Figure S15 show the atomic concentration of Pb(II) ions at the top, middle, and bottom regions of the GO layers after adsorption of $PbCl_2$. As noted in Figure S15b, we observed a similar concentration of Pb(II) ions in the top and middle regions, which indicates uniform adsorption of Pb(II) ions throughout GO membranes. This uniform distribution of Pb(II) ions may be ensured by keeping the pH of the feed solution around 5 to prevent uneven deposition of $Pb(OH)_2$ precipitate on one side of the GO membrane.

https://doi.org/10.1021/jacsau.0c00075
JACS Au 2021, 1, 766−776

Electrochemical Impedance Spectroscopy and Cyclic Voltammetry Measurements

XPS revealed a uniform distribution of Pb(II) across GO, which is attributed to facile diffusion through GO membranes. Theoretical calculations predicted a dependence of the diffusion and adsorption of Pb(II) on GO on O-functional groups. To support these findings, we experimentally investigated Pb(II) diffusion through GO membranes with different concentrations of O groups. Controlling the functional groups present on GO is challenging, but recent studies have shown that the content of hydroxyl/epoxide or carboxyl groups on GO sheets may be modulated by varying the content of water in a modified Hummers synthesis method.[43] Reagents such as ethanol, ethylene glycol, and glycerol may also be used to selectively reduce epoxy groups on GO while hydroxyl and carboxyl groups remain unchanged. Hydrazine hydrate may be used to reduce most oxygen functional groups except for carboxyl groups.[44] GO-containing hydroxyl, epoxy, carbonyl, and carboxyl groups have been shown to lose mainly hydroxyl and epoxy groups during reduction, whereas carboxyl species remain untouched.[45] Informed by these previous works, we hydrothermally reduced GO to prepare samples with different concentrations of O groups. GO and reduced GO (rGO) were immobilized on glassy carbon electrodes, and the adsorption and diffusion of Pb(II) were determined using cyclic voltammetry (CV) and electrochemical impedance spectroscopy (EIS). In addition to the surface O-functionality, the solvated nanopore environment in GO may control diffusion and adsorption.[46] We characterized the surface O-functionality of GO and rGO using XPS. The C 1s spectra presented in Figure S16 indicate lower coverage of O groups in rGO with ∼50% decrease in epoxides and hydroxyls and a ∼12% decrease in carboxyls and carbonyls compared to GO. CV measurements were performed on the GO and rGO electrodes, revealing different double-layer capacitance (Figure S17). The rGO showed a relatively flat capacitive region compared to GO due to increased conductivity[47] and a redox peak at 0.2 V, which may be due to residual redox-active quinones/hydroquinones.[48] Such peaks on GO may be suppressed by lower electrical conductivity. Based on the CV capacitive region, the number of Pb(II) ions in the double-layer region, including inside the pores, was estimated to be 2.6 × 10^{16} and 14 × 10^{16} ions/cm^3 for GO and rGO, respectively. Considering that rGO has a lower coverage of C═O and COOH groups, which may result in lower adsorption capacity, one may expect GO to have more Pb(II) ions. The lower Pb(II) density on GO compared to rGO may be due to initially adsorbed Pb(II) ions that block surface pores, preventing diffusion of further ions into the GO membrane. Without enhanced adsorption of Pb(II) and blocked pores, Pb(II) ions can sieve through rGO and increase the density of ions compared to GO. Increased diffusion rates of cations in GO with fewer O groups has been reported in the literature.[49] Banda et al. showed the increased diffusion of cations in GO sheets with diamine pillars that react with oxygen functional groups and decrease their coverage.[49]

To understand the diffusion of Pb(II) ions at the surface and inside the pores of GO and rGO, EIS measurements were performed from 1 MHz to 1 Hz with a perturbation amplitude of 10 mV. Nyquist plots of the EIS data for GO and rGO electrodes are presented in Figure 5. The high-frequency region (i.e., 1 MHz) of EIS typically represents the polarization of the working electrode controlled by charge transfer kinetics

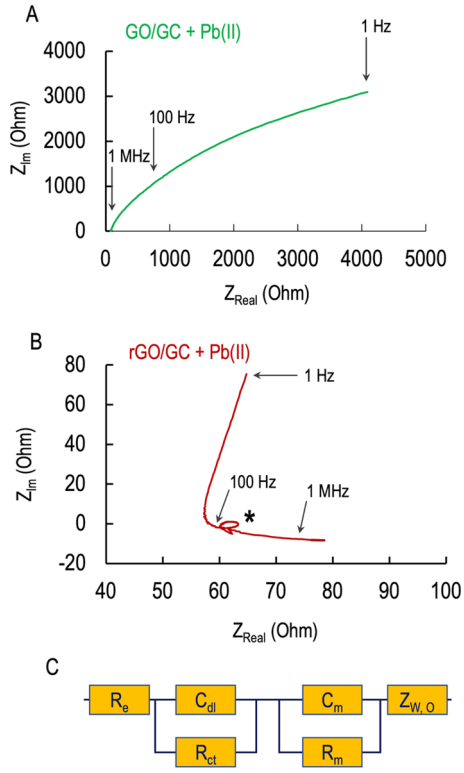

Figure 5. Nyquist plots obtained from EIS measurements of cells containing: (A) GO and (B) rGO. The * marks the inductive loop due to diffusion of ions inside pores. (C) Equivalent circuit model used to fit the EIS data (R_e, electrolyte resistance; R_{ct}, charge transfer resistance; C_{dl}, double-layer capacitance; R_m, resistance inside pores; C_m, double-layer capacitance derived at membrane pores; $Z_{w,o}$, Warburg impedance).

involving adsorption/desorption of electrolyte ions to and from the double-layer region. The lower frequency region (i.e., 100−1 Hz) represents the polarization of the electrode controlled by diffusion of ions through pores of layered GO and rGO. Compared to GO, the rGO electrodes showed an inductive loop due to relaxed diffusion of ions inside the pores. This observation confirms our hypothesis, based on CV, that Pb(II) ions are sieving through rGO laminates. Based on our EIS and CV observations, we postulate that the diffusion of ions and distortion of the double layer were facilitated by reduction of surface O groups in rGO. These observations agree with the theoretical prediction of less favorable ion adsorption on rGO. To quantify the diffusion properties, the EIS data were fit with an equivalent circuit model (Figure 5c). The ion diffusion coefficients were determined to be 1.0 × 10^{-5} and 1.3 × 10^{-5} cm^2/s for GO and rGO, respectively. These values are consistent with the theoretical predictions: on low O-content graphene oxides (rGO), the diffusion coefficient is higher than that on high O-content graphene oxides (GO). Specifically, the diffusion coefficient is 0.25 (×10^{-5} cm^2/s) and 0.14 on O-graphene and HO-graphene, respectively, whereas it is 0.06 on HOOC-graphene. See Table S4 for more details. Overall, our combined theoretical and experimental studies indicate that functionalization of GO controls the adsorption/diffusion properties of Pb(II) at water/GO interfaces, which is key to controlling and improving the efficiency of GO membranes for separations and desalination.

https://doi.org/10.1021/jacsau.0c00075
JACS Au 2021, 1, 766−776

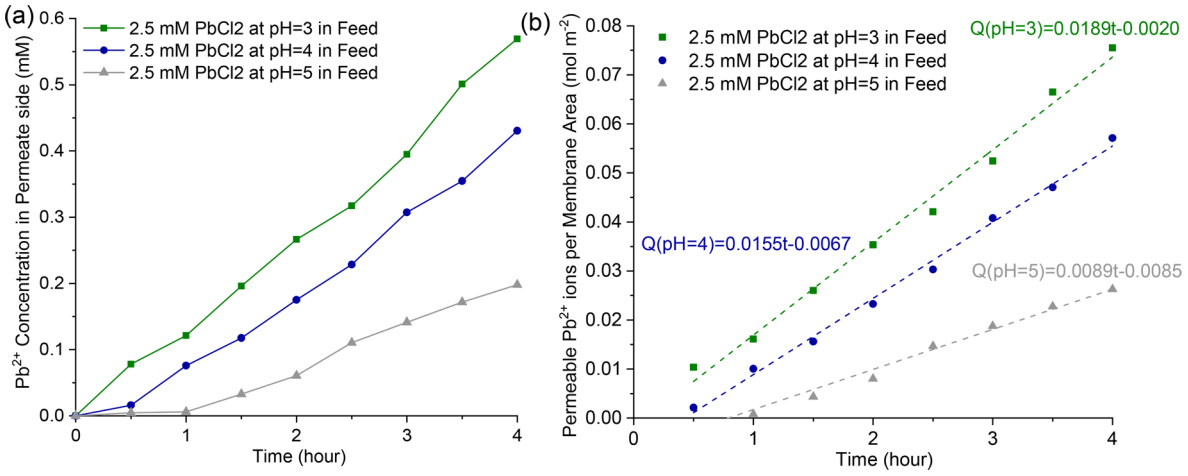

Figure 6. (a) Plot of Pb(II) concentration on the permeate side of the GO membrane versus permeate time at different pH values of the $PbCl_2$ feed solution. (b) Fitted linear equations of permeating Pb(II) ions per GO membrane area versus permeate time at different pH values of the $PbCl_2$ feed solution. The calculated Pb(II) permeation rates and diffusion coefficients at different pH values of the $PbCl_2$ feed solution are provided in Table S5.

Experimental Determination of Reversible Pb(II) Adsorption and Diffusion through Functionalized GO Membranes

In addition to the Pb(II) adsorption experiment, we also used an electrochemical H-cell to investigate the effect of the pH of the $PbCl_2$ feed solution on the permeation of Pb(II) through the GO membrane. By individually keeping different pH values (3, 4, and 5) of the $PbCl_2$ feed solution, the corresponding Pb(II) concentrations on the permeate side at different times were measured using an Pb ISE. The data are plotted in Figure 6a.

The permeation of Pb(II) ions, which is a linear function of permeate time (Figure 6b), was used to calculate the Pb(II) permeation rates and diffusion coefficients based on eq 1 in the Experimental Methods section below. As shown, these two parameters dramatically decreased as the pH of the feed $PbCl_2$ solution increased. Since the *d*-spacing of the GO layers measured with XRD was not substantially changed after adsorption of Pb(II) at different pH values (Figure S18), the effect of the pH of $PbCl_2$ on the permeation of Pb(II) through the GO membranes was mainly attributed to the adsorption of Pb on GO. Specifically, when testing a $PbCl_2$ solution with higher pH in the feed, more Pb(II) ions adsorb onto the GO layers (Figure 4). Consequentially, less Pb(II) permeates through GO membranes, resulting in a lower Pb(II) permeation rate and diffusion coefficient. The diffusion coefficient calculated using the H-cell (D_{CP}) is lower that the values determined using the electrochemical cell (D_{PP}, the Pb(II) diffusion coefficient due to potential polarization). This difference may be due to factors such as an increased concentration of $PbCl_2$ and potential driving force employed during the electrochemical measurements, whereas the diffusion of Pb(II) ions through the ion sieving channels of the GO membrane is driven only by concentration polarization (CP). Moreover, different concentrations of $PbCl_2$ in the feed solution (2.5, 12.5, and 25 mM) were studied, revealing a linear relationship between the Pb(II) permeation rate and concentration of the $PbCl_2$ feed solution. It should be noted that $PbCl_2$ feed solutions at pH = 6 and 7 were not investigated in the permeation experiments since substantial amounts of $Pb(OH)_2$ precipitate would have formed and been concentrated on one side of the GO surface, likely blocking the permeation of Pb(II).

CONCLUSION

We report on a combined theoretical and experimental study of the effects of graphene functionalization on the adsorption behavior of water and Pb(II). Through large AIMD simulations, a detailed picture of the structure at the interface emerges: on HOOC-graphene, Pb(II) forms inner-sphere coordination complexes with a concurrent restructuring of the water interface and the solvation structure of the cation. In contrast, on the HO- and O-graphene, Pb forms outer sphere complexes without further affecting the solvation structure of the cations. Our results indicate that HOOC-graphene shows outstanding adsorption capacity attributed to the deprotonation of the carboxyl groups. This, in turn, suggests that adsorption/desorption can be gated by adjusting the pH, which was validated by subsequent Pb adsorption and diffusion experiments. This work also emphasizes the need for extended molecular models that can imitate the real systems that not only include the adsorption site but also take into account the solvation, desolvation, and reactive events that take place during separation phenomena. FTIR, Raman, and XPS characterization of GO membranes used for $PbCl_2$ filtration at different pH demonstrated the increase in Pb adsorption as a function of pH (3–7). Additional CV and EIS electrochemical measurements on variably reduced GO show that rGO with a lower coverage of O-containing groups allow higher Pb(II) permeability through the membrane. Taken together, these results indicate that HOOC-GO is best suited as an adsorbent rather than as a sieve for Pb(II) separations, and it can be easily regenerated by a simple pH swing. pH-dependent permeation experiments suggest that a pH around 5 is best suited to guarantee significant deprotonation of the COOH groups while avoiding precipitation of $Pb(OH)_2$ at higher pH values. In addition, the low water density at the interfacial layer on HOOC-graphene could potentially impact the water flux in nanochannels of a sieving system, decreasing the separation efficiency. While HO-graphene does not bind Pb(II) as strongly as HOOC-graphene, its ability to form hydrogen bonds with water results in better water penetration, while still

https://doi.org/10.1021/jacsau.0c00075
JACS Au 2021, 1, 766–776

slowing down solvated cations. As a result, O- and HO-graphene may be the best candidates for Pb(II) separation by sieving.

METHODS

Computational Methods

Motivated by open issues mentioned above, we have carried out a state-of-the-art theoretical investigation on the role of functionalization in the interaction of water liquid with GO and in the adsorption of Pb(II) from an aqueous phase on GO. Here, we conducted AIMD simulations using the CP2K program.[50] Interatomic forces were calculated at the PBE-D3 density functional level of theory.[51,52] We employed the hybrid Gaussian plane-wave basis set scheme,[53] in which the molecular optimized double-ζ Gaussian basis sets[54] were used to expand Kohn−Sham orbitals and a plane-wave cutoff of 440 Ry was used to compute electrostatic terms. The norm-conserving pseudopotentials[55] were adopted to describe the core electrons. Only Γ-points were sampled in the self-consistent calculations. The surface dipole correction[56] for asymmetric slabs was applied. Molecular dynamics simulations were carried out within the canonical (NVT) ensemble. The Verlet algorithm[57] for the integration of the equation of motions with the time step of 0.55 fs was used. To equilibrate each system, we adopt the following protocol: starting from a local minimum, a 5 ps run at 330 K was followed with a 15 ps run at 500 K, the system was then annealed for 3 ps to approximately 10 K. Next, a 5 ps 330 K run was conducted. Finally, a 40−50 ps production run at 330 K was used to analyze properties of the system.

While O, OH, and COOH are fundamental functional groups of GO,[5,27,58] for completeness, we also considered H functionalization since in many cases GO operates in an acidic solution where protons are available to interact with an "intact" (unfunctionalized) area of GO. The monovalent species H, OH, and COOH were added to the "top" sites, while the divalent species O was added to the bridge sites of graphene sheets. To stabilize the monovalent species on graphene, for each functional group, we added one more H atom to the opposite side of the graphene to saturate unpaired π electrons of the carbon surface.[59] Functional coverage effects were examined through three coverages: 0 monolayer (pristine graphene, no functional group), 0.125 monolayer (one functional group on every 8 graphene atoms), and 0.0625 monolayer. A (8 × 4) rectangular graphene 2D unit cell (~19.8 × 17.1 Å^2, containing 128 C atoms) was adopted see Figure S1 in the Supporting Information. Although in GO functional groups are randomly distributed[60] and the local structure of GO is rather complicated,[61] for the purpose of this study, we adopted a uniformly distributed pattern of functional groups. Each GO thin film supports 180 water molecules. We then added one Pb cation and two counterions of Cl to an equilibrated frame from systems that contain only water and surfaces.

The density (g/cm^3) as a function of the distance to the carbon surface is given by $\rho(z) = \frac{\langle n(z)\rangle}{dV}m$, where $\frac{\langle n(z)\rangle}{dV}$ is the average number of water molecules per volume unit between two planes, parallel to graphene, at z + dz relative to the carbon plane, and m is the mass of a water molecule.

We defined the hydrogen bond between two water molecules OH···O HB by two parameters, the O−O distance (<3.5 Å) and the ∠HOO angle (<30°) based on a work by Luzar and Chandler.[62]

Experimental Methods

The adsorption and diffusion of Pb(II) ions in GO membranes with different surface functional groups were studied by conducting filtration experiments at different pH values and electrochemical experiments with two different concentrations of surface O groups, respectively.

Pb(II) Adsorption−Filtration Experiments

In order to experimentally characterize the interaction between −COOH groups on GO and Pb(II) ions, as well as the effect of deprotonation of −COOH on Pb(II) adsorption, filtration experiments were performed by passing aqueous lead chloride ($PbCl_2$) solutions with different pH through GO membranes. Specifically, the GO membranes were formed by vacuum-filtering 50 mL of a 0.01 mg/mL GO suspension in water through a polyvinylidene fluoride (PVDF, 47 mm diameter, 0.45 μm pore size, Millipore) support substrate, followed by addition of 50 mL of a 0.25 mM aqueous lead chloride solution ($PbCl_2$, Sigma-Aldrich) with a predetermined pH value. After filtration, 50 mL of deionized water was passed through the membranes to remove non- or weakly bonded Pb(II) ions from the hydrated membrane, which was then vacuum-dried over 48 h at room temperature. Solutions of 1 M hydrochloric acid (HCl) or 0.1 M ammonia hydroxide (NH_4OH) were used to adjust the pH of the $PbCl_2$ solutions, which were measured using a Thermo Scientific Orion Star Benchtop pH meter. All of the membranes, including the neat GO membrane and the GO membranes with adsorbed Pb(II) at different pH, were characterized by FTIR spectroscopy, Raman spectroscopy, and X-ray photoelectron spectroscopy. Specifically, around 0.5 mg of GO was peeled from the PVDF substrate and mixed with 100 mg of KBr, which was pressed into 8 mm diameter pellets for FTIR analysis. The FTIR spectra (4000−800 cm^{-1}) were recorded with a resolution of 2 cm^{-1} and 1500 scans per sample using a Bruker Vertex 70 FTIR spectrometer (Bruker Optics, Billerica, MA). Background FTIR spectra were collected using pure KBr pellets. Raman spectroscopy was also carried out by passing the output of a 633 nm excitation laser through a tube lens and onto the samples. The backscattered light was collected through the same tube lens, filtered through a dichroic beamsplitter/long-pass filter assembly, and fiber-coupled to a spectrometer charge-coupled device detection system (Andor, Shamrock 303i and iDus 416). Low laser power (<5 mW) and long exposure times (15 min) were used to prevent radiation damage to the samples and suppress fluorescence noise, respectively. The presence of different surface functional groups on GO and rGO was characterized using X-ray photoelectron spectroscopy. The C 1s XPS spectra were collected using a Kratos Axis Ultra DLD spectrometer with a high-performance Al Kα monochromatic X-ray source (1486.6 eV) and a high-resolution hemispherical analyzer. The power of the X-ray source was set at 150 W. Emitted photoelectrons were collected using a detector aligned normal to the sample surface. Data were collected from a 700 × 300 μm^2 area with a pass energy of 40 eV. Charge neutralization was achieved using low-energy electrons (<2 eV). The data were analyzed using the Casa XPS software. All data were peak-corrected to a C 1s binding energy of 285 eV. The XPS peaks were fit using a Gaussian−Lorentzian (GL30) peak shape after performing a Shirley background subtraction. The assignment of the C 1s peaks is based on energy values reported in the literature.[63−66]

Determination of the Diffusion of Pb(II) Ions through GO Membranes

Electrochemical methods, such as cyclic voltammetry and electrochemical impedance spectroscopy were performed on GO and rGO and followed by postcharacterization using XPS. A commercially available GO water dispersion (25 mg/mL) was purchased from MSE Supplies. To synthesize rGO, a stable dispersion of GO at a concentration of 1.67 mg/mL was prepared by adding deionized water to the concentrated GO dispersion and sonicating it for 30 min. The resulting GO suspension was transferred to a Teflon-lined acid digestion vessel (4749, Parr Instrument Company) and hydrothermally reduced by heating the vessel in an oven at 160 °C for 6 h.[65] The hydrothermal treatment resulted in the formation of hydrophobic rGO aggregates. The aggregates were removed from the water and redispersed in acetonitrile to a final concentration of ~1.67 mg/mL. Analysis of the GO and rGO by XPS revealed that the C/O ratio increased from 2.0 to 6.6 following hydrothermal reduction of the GO.[67] Separate electrodes were prepared by drop-casting approximately 20 μL of GO and 30 μL of rGO suspensions in acetonitrile on glassy carbon (GC) surfaces. SIGRADUR G plates (10 mm × 10 mm × 4 mm, one side diamond polished) purchased from HTW Hochtemperatur-Werkstoffe GmbH were used as GC working electrodes. The drop-cast solutions were dried under vacuum at

https://doi.org/10.1021/jacsau.0c00075
JACS Au 2021, 1, 766−776

room temperature for an hour. The volume of the drop-cast solutions was varied to achieve a similar dried mass loading of 50 μg on both the GO and rGO immobilized electrodes. The dried electrodes were used as the working electrodes in the electrochemical measurements. To characterize the properties of Pb(II) in GO and rGO, CV and EIS experiments were used to determine the adsorption and transport properties of the prepared electrodes using Versastat 3 (Princeton Applied Research, Oakridge, TN). Note that the presence of a thin layer of GO or rGO creates a membrane−electrode interface, allowing us to study the transport properties inside the porous region. These results can be compared to the diffusion properties derived from theoretical calculations. Electrochemical cells were constructed using GC as the working electrodes, platinum as the counter electrodes, and silver wires as the reference electrodes. A 10 mM solution of $PbCl_2$ dissolved in deionized water was used as a model electrolyte. To determine the charges and double-layer adsorption behavior on the layered GC electrodes, CV measurements were made between −0.2 and +0.7 V. EIS experiments were also performed to examine the diffusional resistance inside the pores of the GO layers. In EIS, a sinusoidal perturbation with an amplitude of 10 mV and frequency over a range of 1 MHz to 1 Hz is applied across the electrochemical cell and the impedance across the circuit is measured as a function of the frequency.

pH Effects on Pb(II) Permeation Experiments

We used an electrochemical H-cell (redox.me) to investigate the effect of the pH of the $PbCl_2$ feed solution on the permeation of Pb(II) through GO membranes. The Pb-ion-selective electrode (ISE) (Orion Lead Electrode, model 9682BNWP, Thermo Fisher Scientific)[68,69] was used to measure the concentration of Pb(II) on the permeate side of the GO membranes. Before the measurements, several standard $PbCl_2$ solutions with specific concentrations (0.05, 0.25, 1.25, and 2.5 mM) were prepared separately to calibrate the Pb(II) ISE. Specifically, 5 mL of HCl solution with pH = 4 was used as the background electrolyte to maintain constant ionic strength. One hundred microliter aliquots of a $PbCl_2$ standard solution were sequentially added to achieve specific Pb(II) concentrations of 1×10^{-6}, 5×10^{-6}, 1×10^{-5}, and 5×10^{-5} M. The Pb ISE was used to record the potential of each solution to generate a linear calibration plot of Pb(II) concentration versus potential. During the measurements, 2.5 mM $PbCl_2$ with a certain pH and deionized water were used as the feed and permeate solutions, respectively. A 100 μL aliquot was taken every 30 min from the permeate side of the GO membrane and added into 5 mL of HCl solution with pH = 4 to be measured using the Pb ISE. The Pb(II) concentration was recorded versus time, and the data were used to generate a linear plot. According to eq 1, the slope and x-axis intercept of the linear equation may be used to calculate the Pb(II) permeation rate and diffusion coefficient:[70,71]

$$Q_t = P\left(t - \frac{l^2}{6D_{CP}}\right) \quad (1)$$

In eq 1, Q_t (mol m^{-2}) is the total amount of permeate Pb(II) ions per unit surface area of GO membrane, t (h) is the Pb(II) permeation time, P (mol m^{-2} h^{-1}) is the permeation rate of Pb(II), l is the thickness of the GO membrane (125 μm), and D_{CP} (cm^2 s^{-1}) is the Pb(II) diffusion coefficient due to concentration polarization.

ASSOCIATED CONTENT

Supporting Information

The Supporting Information is available free of charge at https://pubs.acs.org/doi/10.1021/jacsau.0c00075.

Unit cells; potential of the mean force; coordination number; orientation of water molecules; water transport in the first layer; polarizability and forces of the first layer water; Pb(II) on GO and Pb(II) in water box; coordination number of Pb(II); bonding charge density; H_3O^+ species; Pb(II) diffusion coefficients; H_3O^+ species; vibration spectra; experimental characterization of adsorbed Pb on GO and reduced GO (PDF)

AUTHOR INFORMATION

Corresponding Authors

Vassiliki-Alexandra Glezakou − *Physical and Computational Sciences Directorate, Pacific Northwest National Laboratory, Richland, Washington 99352, United States;* orcid.org/0000-0001-6028-7021; Email: Vanda.Glezakou@pnnl.gov

Grant E. Johnson − *Physical and Computational Sciences Directorate, Pacific Northwest National Laboratory, Richland, Washington 99352, United States;* orcid.org/0000-0003-3352-4444; Email: Grant.Johnson@pnnl.gov

Authors

Manh-Thuong Nguyen − *Physical and Computational Sciences Directorate, Pacific Northwest National Laboratory, Richland, Washington 99352, United States*

Jun Zhang − *Physical and Computational Sciences Directorate, Pacific Northwest National Laboratory, Richland, Washington 99352, United States;* orcid.org/0000-0001-9093-9430

Venkateshkumar Prabhakaran − *Physical and Computational Sciences Directorate, Pacific Northwest National Laboratory, Richland, Washington 99352, United States;* orcid.org/0000-0001-6692-6488

Shuai Tan − *Physical and Computational Sciences Directorate, Pacific Northwest National Laboratory, Richland, Washington 99352, United States*

Eric T. Baxter − *Physical and Computational Sciences Directorate, Pacific Northwest National Laboratory, Richland, Washington 99352, United States*

Vaithiyalingam Shutthanandan − *Physical and Computational Sciences Directorate, Pacific Northwest National Laboratory, Richland, Washington 99352, United States;* orcid.org/0000-0003-2957-7535

Roger Rousseau − *Physical and Computational Sciences Directorate, Pacific Northwest National Laboratory, Richland, Washington 99352, United States;* orcid.org/0000-0003-1947-0478

Complete contact information is available at: https://pubs.acs.org/10.1021/jacsau.0c00075

Notes

The authors declare no competing financial interest.

ACKNOWLEDGMENTS

This work was supported by the U.S. Department of Energy (DOE), Office of Science, Office of Basic Energy Sciences, Chemical Sciences, Geosciences, and Biosciences Division, project 72353 (Interfacial Structure and Dynamics in Ion Separations). Part of this work was performed using EMSL, a national scientific user facility sponsored by the DOE's Office of Biological and Environmental Research and located at Pacific Northwest National Laboratory (PNNL). PNNL is a multiprogram national laboratory operated for DOE by Battelle for the U.S. Department of Energy under Contract DE-AC05-76RL01830. Computer resources were provided by Research Computing at Pacific Northwest National Laboratory, and the National Energy Research Scientific Computing Center (NERSC), a U.S. Department of Energy Office of

Science User Facility operated under Contract No. DE-AC02-05CH11231.

REFERENCES

(1) He, Y.; Wu, P.; Xiao, W.; Li, G.; Yi, J.; He, Y.; et al. Efficient removal of Pb(II) from aqueous solution by a novel ion imprinted magnetic biosorbent: Adsorption kinetics and mechanisms. *PLoS One* **2019**, *14* (3), No. e0213377.

(2) La, D. D.; Thi, H. P. N.; Nguyen, T. A.; Bhosale, S. V. Effective removal of Pb(ii) using a graphene@ternary oxides composite as an adsorbent in aqueous media. *New J. Chem.* **2017**, *41* (23), 14627−14634.

(3) Yu, C.; Shao, Z.; Hou, H. A functionalized metal−organic framework decorated with O- groups showing excellent performance for lead(ii) removal from aqueous solution. *Chemical Science* **2017**, *8* (11), 7611−7619.

(4) Pietrucci, F.; Boero, M.; Andreoni, W. How natural materials remove heavy metals from water: mechanistic insights from molecular dynamics simulations. *Chemical Science* **2021**, *12*, 2979.

(5) Perreault, F.; Fonseca de Faria, A.; Elimelech, M. Environmental applications of graphene-based nanomaterials. *Chem. Soc. Rev.* **2015**, *44* (16), 5861−5896.

(6) Peng, W. J.; Li, H. Q.; Liu, Y. Y.; Song, S. X. A review on heavy metal ions adsorption from water by graphene oxide and its composites. *J. Mol. Liq.* **2017**, *230*, 496−504.

(7) Kim, H. W.; Yoon, H. W.; Yoon, S. M.; Yoo, B. M.; Ahn, B. K.; Cho, Y. H.; et al. Selective Gas Transport Through Few-Layered Graphene and Graphene Oxide Membranes. *Science* **2013**, *342* (6154), 91−95.

(8) Dahanayaka, M.; Liu, B.; Srikanth, N.; Zhou, K. Ionised graphene oxide membranes for seawater desalination. *Desalination* **2020**, *496*, 114637.

(9) Ahmadi, H.; Hosseini, E.; Cha-Umpong, W.; Abdollahzadeh, M.; Korayem, A. H.; Razmjou, A.; Chen, V.; Asadnia, M. Incorporation of Natural Lithium-Ion Trappers into Graphene Oxide Nanosheets. *Adv. Mater. Technol.* **2020**, 2000665.

(10) Joshi, R. K.; Carbone, P.; Wang, F. C.; Kravets, V. G.; Su, Y.; Grigorieva, I. V.; et al. Precise and Ultrafast Molecular Sieving Through Graphene Oxide Membranes. *Science* **2014**, *343* (6172), 752−754.

(11) Gogotsi, Y. Moving ions confined between graphene sheets. *Nat. Nanotechnol.* **2018**, *13* (8), 625−627.

(12) Cha-Umpong, W.; Hosseini, E.; Razmjou, A.; Zakertabrizi, M.; Korayem, A. H.; Chen, V. New molecular understanding of hydrated ion trapping mechanism during thermally-driven desalination by pervaporation using GO membrane. *J. Membr. Sci.* **2020**, *598*, 117687.

(13) Montes-Navajas, P.; Asenjo, N. G.; Santamaria, R.; Menendez, R.; Corma, A.; Garcia, H. Surface Area Measurement of Graphene Oxide in Aqueous Solutions. *Langmuir* **2013**, *29* (44), 13443−13448.

(14) You, Y.; Sahajwalla, V.; Yoshimura, M.; Joshi, R. K. Graphene and graphene oxide for desalination. *Nanoscale* **2016**, *8* (1), 117−119.

(15) Mi, B. Graphene oxide membranes for ionic and molecular sieving. *Science* **2014**, *343* (6172), 740−742.

(16) Li, X. H.; Wang, Z.; Li, Q.; Ma, J. X.; Zhu, M. Z. Preparation, characterization, and application of mesoporous silica-grafted graphene oxide for highly selective lead adsorption. *Chem. Eng. J.* **2015**, *273*, 630−637.

(17) Dimiev, A. M., Eigler, S., Eds. *Graphene Oxide: Fundamentals and Applications*; John Wiley & Sons, Ltd., 2017.

(18) Taherian, F.; Marcon, V.; van der Vegt, N. F. A.; Leroy, F. What Is the Contact Angle of Water on Graphene? *Langmuir* **2013**, *29* (5), 1457−1465.

(19) Cote, L. J.; Cruz-Silva, R.; Huang, J. X. Flash Reduction and Patterning of Graphite Oxide and Its Polymer Composite. *J. Am. Chem. Soc.* **2009**, *131* (31), 11027−11032.

(20) Mouhat, F.; Coudert, F. X.; Bocquet, M. L. Structure and chemistry of graphene oxide in liquid water from first principles. *Nat. Commun.* **2020**, *11* (1), 1566.

(21) Nguyen, M. T.; Phong, P. N. Accelerating Dynamics of H on Graphene by Coadsorbates. *J. Phys. Chem. A* **2017**, *121* (29), 5520−5523.

(22) Ambrosetti, A.; Silvestrelli, P. L. Adsorption of Rare-Gas Atoms and Water on Graphite and Graphene by van der Waals-Corrected Density Functional Theory. *J. Phys. Chem. C* **2011**, *115* (9), 3695−3702.

(23) Chen, L. H.; Guo, Y. A.; Xu, Z. J.; Yang, X. N. Multiscale Simulation of the Interaction and Adsorption of Ions on a Hydrophobic Graphene Surface. *ChemPhysChem* **2018**, *19* (21), 2954−2960.

(24) Dobrota, A. S.; Pasti, I. A.; Mentus, S. V.; Skorodumova, N. V. A general view on the reactivity of the oxygen-functionalized graphene basal plane. *Phys. Chem. Chem. Phys.* **2016**, *18* (9), 6580−6586.

(25) Yang, S. T.; Chang, Y. L.; Wang, H. F.; Liu, G. B.; Chen, S.; Wang, Y. W.; et al. Folding/aggregation of graphene oxide and its application in Cu2+ removal. *J. Colloid Interface Sci.* **2010**, *351* (1), 122−127.

(26) Huang, Z. H.; Zheng, X. Y.; Lv, W.; Wang, M.; Yang, Q. H.; Kang, F. Y. Adsorption of Lead(II) Ions from Aqueous Solution on Low-Temperature Exfoliated Graphene Nanosheets. *Langmuir* **2011**, *27* (12), 7558−7562.

(27) Dreyer, D. R.; Park, S.; Bielawski, C. W.; Ruoff, R. S. The chemistry of graphene oxide. *Chem. Soc. Rev.* **2010**, *39* (1), 228−240.

(28) Wang, X. X.; Chen, Z. S.; Yang, S. B. Application of graphene oxides for the removal of Pb(II) ions from aqueous solutions: Experimental and DFT calculation. *J. Mol. Liq.* **2015**, *211*, 957−964.

(29) Zhao, G. X.; Li, J. X.; Ren, X. M.; Chen, C. L.; Wang, X. K. Few-Layered Graphene Oxide Nanosheets As Superior Sorbents for Heavy Metal Ion Pollution Management. *Environ. Sci. Technol.* **2011**, *45* (24), 10454−10462.

(30) Yoon, Y.; Rousseau, R.; Weber, R. S.; Mei, D. H.; Lercher, J. A. First-Principles Study of Phenol Hydrogenation on Pt and Ni Catalysts in Aqueous Phase. *J. Am. Chem. Soc.* **2014**, *136* (29), 10287−10298.

(31) Xian, S. K.; Peng, J. J.; Zhang, Z. J.; Xia, Q. B.; Wang, H. H.; Li, Z. Highly enhanced and weakened adsorption properties of two MOFs by water vapor for separation of CO2/CH4 and CO2/N-2 binary mixtures. *Chem. Eng. J.* **2015**, *270*, 385−392.

(32) Marcus, Y. Thermodynamics of Solvation of Ions.5. Gibbs Free-Energy of Hydration at 298.15-K. *J. Chem. Soc., Faraday Trans.* **1991**, *87* (18), 2995−2999.

(33) Kang, K. M.; Kim, D. W.; Ren, C. E.; Cho, K. M.; Kim, S. J.; Choi, J. H.; et al. Selective Molecular Separation on Ti3C2Tx−Graphene Oxide Membranes during Pressure-Driven Filtration: Comparison with Graphene Oxide and MXenes. *ACS Appl. Mater. Interfaces* **2017**, *9* (51), 44687−44694.

(34) Zheng, S. X.; Tu, Q. S.; Urban, J. J.; Li, S. F.; Mi, B. X. Swelling of Graphene Oxide Membranes in Aqueous Solution: Characterization of Interlayer Spacing and Insight into Water Transport Mechanisms. *ACS Nano* **2017**, *11* (6), 6440−6450.

(35) Tocci, G.; Joly, L.; Michaelides, A. Friction of water on graphene and hexagonal boron nitride from ab initio methods: very different slippage despite very similar interface structures. *Nano Lett.* **2014**, *14* (12), 6872−6877.

(36) Wei, N.; Peng, X. S.; Xu, Z. P. Breakdown of fast water transport in graphene oxides. *Phys. Rev. E* **2014**, *89* (1), 012113.

(37) Guardia, E.; Skarmoutsos, I.; Masia, M. Hydrogen Bonding and Related Properties in Liquid Water: A Car-Parrinello Molecular Dynamics Simulation Study. *J. Phys. Chem. B* **2015**, *119* (29), 8926−8938.

(38) Mecozzi, S.; West, A. P.; Dougherty, D. A. Cation-pi interactions in simple aromatics: Electrostatics provide a predictive tool. *J. Am. Chem. Soc.* **1996**, *118* (9), 2307−2308.

(39) Gagné, O. C.; Hawthorne, F. C. Bond-length distributions for ions bonded to oxygen: metalloids and post-transition metals. *Acta Crystallogr., Sect. B: Struct. Sci., Cryst. Eng. Mater.* **2018**, *74* (1), 63−78.

(40) Park, S.; Lee, K.-S.; Bozoklu, G.; Cai, W.; Nguyen, S. T.; Ruoff, R. S. Graphene oxide papers modified by divalent ions - Enhancing

https://doi.org/10.1021/jacsau.0c00075
JACS Au 2021, 1, 766−776

mechanical properties via chemical cross-linking. *ACS Nano* **2008**, *2* (3), 572−578.
(41) Ni, Z. H.; Yu, T.; Lu, Y. H.; Wang, Y. Y.; Feng, Y. P.; Shen, Z. X. Uniaxial Strain on Graphene: Raman Spectroscopy Study and Band-Gap Opening. *ACS Nano* **2008**, *2* (11), 2301−2305.
(42) Xu, D.; Tan, X. L.; Chen, C. L.; Wang, X. K. Removal of Pb(II) from aqueous solution by oxidized multiwalled carbon nanotubes. *J. Hazard. Mater.* **2008**, *154* (1−3), 407−416.
(43) Chen, J.; Zhang, Y.; Zhang, M.; Yao, B.; Li, Y.; Huang, L.; et al. Water-enhanced oxidation of graphite to graphene oxide with controlled species of oxygenated groups. *Chemical Science* **2016**, *7* (3), 1874−1881.
(44) Xu, C.; Yuan, R.-S.; Wang, X. Selective reduction of graphene oxide. *New Carbon Materials* **2014**, *29* (1), 61−66.
(45) Haubner, K.; Murawski, J.; Olk, P.; Eng, L. M.; Ziegler, C.; Adolphi, B.; et al. The route to functional graphene oxide. *ChemPhysChem* **2010**, *11* (10), 2131−2139.
(46) Su, P.; Wang, F.; Li, Z.; Tang, C. Y.; Li, W. Graphene oxide membranes: controlling their transport pathways. *J. Mater. Chem. A* **2020**, *8*, 15319−15340.
(47) Dubin, S.; Gilje, S.; Wang, K.; Tung, V. C.; Cha, K.; Hall, A. S.; et al. A one-step, solvothermal reduction method for producing reduced graphene oxide dispersions in organic solvents. *ACS Nano* **2010**, *4* (7), 3845−3852.
(48) Shao, Y.; Wang, J.; Engelhard, M.; Wang, C.; Lin, Y. Facile and controllable electrochemical reduction of graphene oxide and its applications. *J. Mater. Chem.* **2010**, *20* (4), 743−748.
(49) Banda, H.; Périé, S.; Daffos, B.; Dubois, L.; Crosnier, O.; Simon, P.; et al. Investigation of ion transport in chemically tuned pillared graphene materials through electrochemical impedance analysis. *Electrochim. Acta* **2019**, *296*, 882−890.
(50) VandeVondele, J.; Krack, M.; Mohamed, F.; Parrinello, M.; Chassaing, T.; Hutter, J. QUICKSTEP: Fast and accurate density functional calculations using a mixed Gaussian and plane waves approach. *Comput. Phys. Commun.* **2005**, *167* (2), 103−128.
(51) Perdew, J. P.; Burke, K.; Ernzerhof, M. Generalized gradient approximation made simple. *Phys. Rev. Lett.* **1996**, *77* (18), 3865−3868.
(52) Grimme, S.; Antony, J.; Ehrlich, S.; Krieg, H. A consistent and accurate ab initio parametrization of density functional dispersion correction (DFT-D) for the 94 elements H-Pu. *J. Chem. Phys.* **2010**, *132* (15), 154104.
(53) Lippert, G.; Hutter, J.; Parrinello, M. A hybrid Gaussian and plane wave density functional scheme. *Mol. Phys.* **1997**, *92* (3), 477−487.
(54) VandeVondele, J.; Hutter, J. Gaussian basis sets for accurate calculations on molecular systems in gas and condensed phases. *J. Chem. Phys.* **2007**, *127* (11), 114105.
(55) Goedecker, S.; Teter, M.; Hutter, J. Separable dual-space Gaussian pseudopotentials. *Phys. Rev. B: Condens. Matter Mater. Phys.* **1996**, *54* (3), 1703−1710.
(56) Bengtsson, L. Dipole correction for surface supercell calculations. *Phys. Rev. B: Condens. Matter Mater. Phys.* **1999**, *59* (19), 12301−12304.
(57) Verlet, L. Computer Experiments on Classical Fluids.I. Thermodynamical Properties of Lennard-Jones Molecules. *Phys. Rev.* **1967**, *159* (1), 98.
(58) Singh, R. K.; Kumar, R.; Singh, D. P. Graphene oxide: strategies for synthesis, reduction and frontier applications. *RSC Adv.* **2016**, *6* (69), 64993−65011.
(59) Erni, R.; Rossell, M. D.; Nguyen, M.-T.; Blankenburg, S.; Passerone, D.; Hartel, P.; Alem, N.; Erickson, K.; Gannett, W.; Zettl, A. Stability and dynamics of small molecules trapped on graphene. *Phys. Rev. B: Condens. Matter Mater. Phys.* **2010**, *82*, 165443.
(60) Nguyen, M. T.; Erni, R.; Passerone, D. Two-dimensional nucleation and growth mechanism explaining graphene oxide structures. *Phys. Rev. B: Condens. Matter Mater. Phys.* **2012**, *86* (11), 115406.
(61) Erickson, K.; Erni, R.; Lee, Z.; Alem, N.; Gannett, W.; Zettl, A. Determination of the Local Chemical Structure of Graphene Oxide and Reduced Graphene Oxide. *Adv. Mater.* **2010**, *22* (40), 4467−4472.
(62) Luzar, A.; Chandler, D. Structure and Hydrogen-Bond Dynamics of Water-Dimethyl Sulfoxide Mixtures by Computer-Simulations. *J. Chem. Phys.* **1993**, *98* (10), 8160−8173.
(63) Yang, D.; Velamakanni, A.; Bozoklu, G.; Park, S.; Stoller, M.; Piner, R. D.; et al. Chemical analysis of graphene oxide films after heat and chemical treatments by X-ray photoelectron and Micro-Raman spectroscopy. *Carbon* **2009**, *47* (1), 145−152.
(64) Yumitori, S. Correlation of C1s chemical state intensities with the O1s intensity in the XPS analysis of anodically oxidized glass-like carbon samples. *J. Mater. Sci.* **2000**, *35* (1), 139−146.
(65) Huang, H.-H.; Joshi, R. K.; De Silva, K. K. H.; Badam, R.; Yoshimura, M. Fabrication of reduced graphene oxide membranes for water desalination. *J. Membr. Sci.* **2019**, *572*, 12−19.
(66) Stobinski, L.; Lesiak, B.; Malolepszy, A.; Mazurkiewicz, M.; Mierzwa, B.; Zemek, J.; et al. Graphene oxide and reduced graphene oxide studied by the XRD TEM and electron spectroscopy methods. *J. Electron Spectrosc. Relat. Phenom.* **2014**, *195*, 145−154.
(67) Krishnamoorthy, K.; Veerapandian, M.; Yun, K.; Kim, S. J. The chemical and structural analysis of graphene oxide with different degrees of oxidation. *Carbon* **2013**, *53*, 38−49.
(68) Babyak, C.; Smart, R. B. Electrochemical Detection of Trace Concentrations of Cadmium and Lead with a Boron-Doped Diamond Electrode: Effect of KCl and KNO3 Electrolytes, Interferences and Measurement in River Water. *Electroanalysis* **2004**, *16* (3), 175−182.
(69) Tang, X.; Wang, P.-Y.; Buchter, G. Ion-selective electrodes for detection of lead (II) in drinking water: A mini-review. *Environments* **2018**, *5* (9), 95.
(70) Crank, J. *The Mathematics of Diffusion*; Oxford University Press, 1979.
(71) Dudek, G.; Borys, P. A simple methodology to estimate the diffusion coefficient in pervaporation-based purification experiments. *Polymers* **2019**, *11* (2), 343.

https://doi.org/10.1021/jacsau.0c00075
JACS Au 2021, 1, 766−776